Supporting Information

Englander et al. 10.1073/pnas.1424712112

SI Experimental Procedures

Purification of Ribosomes, Translation Factors, tRNA Synthetases, tRNAs, and mRNAs. Tightly coupled *Escherichia coli* 70S ribosomes were purified using sucrose density gradient ultracentrifugation as previously described (1, 2) and then stored in a buffer containing 10 mM Tris-acetate ($pH_{25\ °C}$ = 7.5), 60 mM ammonium chloride, 7.5 mM magnesium acetate, 0.5 mM ethylenediamine tetraacetic acid, 6 mM 2-mercaptoethanol, and 40% (vol/vol) sucrose at –80 °C (2, 3). Initiation factors (IFs) 1, 2, and 3; EFs Tu, Ts, and G; formylmethionyl-tRNA formyltransferase; and methionyl-tRNA synthetase were purified as previously described (2, 4). A phenylalanyl-tRNA synthetase containing a six-histidine (6×His) tag at its N terminus and a threonine to glycine mutation at position 251 (T251G) was obtained from an overexpression strain kindly provided by David Tirrell (California Institute of Technology, Pasadena, CA) (5). This mutant phenylalanyl-tRNA synthetase was purified over a Ni^{2+}-nitrilotriacetic acid (NTA) column (Novagen) and aminoacylated Phe onto $tRNA^{Phe}$ with ∼95% efficiency. Lysyl-tRNA synthetase containing a 6×His tag was obtained from an overexpression strain kindly provided by Takuya Ueda (University of Tokyo, Tokyo, Japan) (6) and purified over a Ni^{2+}-NTA column. The Lysyl-tRNA synthetase aminoacylated Lys onto $tRNA^{Lys}$ with ∼35% efficiency.

All tRNAs used in this study ($tRNA^{fMet}$, $tRNA^{Phe}$, $tRNA^{Lys}$, $tRNA^{Val}$, and $tRNA^{Glu}$) were purified from *E. coli* and were purchased from either Sigma or MP Biomedicals. Because control dipeptide synthesis reactions (*Peptide Synthesis Reactions Involving D/L-Phe-tRNAPhe and D/L-Val-tRNAVal*) with $tRNA^{Val}$ demonstrated that this tRNA, as purchased from Sigma, was significantly acylated, $tRNA^{Val}$ was deacylated by incubation in 1.8 M Tris·hydrochloride ($pH_{25\ °C}$ = 8) for 3 h at 37 °C (7) before aminoacylating with D-Val (Fig. S2*A*). Control dipeptide synthesis reactions with $tRNA^{Phe}$ and $tRNA^{Lys}$ did not yield any dipeptide product, and consequently, these tRNAs were used without deacylation.

mRNA templates were in vitro transcribed using T7 RNA polymerase and double-stranded DNA templates encoding variants of the bacteriophage T4 gene product 32 (hereafter referred to as T4gp32) using a protocol described previously (2, 4) and were purified by filtration through an Amicon Centrifugation filter (10,000 MW cutoff) (4). For all experiments except the primer extension inhibition, or toeprinting, assay (*Primer Extension Inhibition, or Toeprinting, Reactions*), truncated T4gp32 mRNAs encoding the first 20 amino acids were used ($T4gp32_{1–20}$). For toeprinting experiments, a longer T4gp32 mRNA encoding the first 224 amino acids was used ($T4gp32_{1–224}$) (4). The specific sequence and length of each T4gp32 mRNA is noted for each experiment described below.

Aminoacylation of tRNAs. Aminoacylation of initiator $tRNA^{fMet}$ and formylation of [^{35}S]-methionyl-$tRNA^{fMet}$ or nonradiolabeled methionyl-$tRNA^{fMet}$ were performed using methionyl-tRNA synthetase and formylmethionyl-tRNA formyltransferase, respectively, following a protocol described previously (2, 4). For the peptide synthesis reactions in Figs. 1 and 2 and Figs. S3 and S4 as well as those described in *Peptide Synthesis Reactions Involving D/L-Phe-$tRNA^{Phe}$ and D/L-Val-$tRNA^{Val}$* and *Peptide Synthesis Reactions Involving D/L-Lys-$tRNA^{Lys}$*, D/L-aminoacyl-tRNAs prepared using either the eFx or the dFx variant of an aminoacyl-tRNA synthetase ribozyme (8) were used to decode the second codon in the mRNA. The eFx ribozyme along with D/L-Phe cyanomethyl esters and the dFx ribozyme along with D/L-Lys or D/L-Val dinitrobenzyl esters were used to aminoacylate $tRNA^{Phe}$, $tRNA^{Lys}$, and $tRNA^{Val}$, respectively, as described by Suga and coworkers (8). The aminoacylation reactions contained 20 μM tRNA, 20 μM dFx or eFx, and 5 mM amino acid–dinitrobenzyl esters or cyanomethyl esters substrate in a buffer of 0.1 M Hepes-K ($pH_{25\ °C}$ = 7.5), 0.1 M potassium chloride, 600 mM magnesium chloride, and 20% dimethyl sulfoxide (8). Aminoacylations of $tRNA^{Phe}$ and $tRNA^{Lys}$ with D/L-Phe and D/L-Lys, respectively, were run for 2 h on ice; aminoacylation of $tRNA^{Val}$ with D/L-Val reaction was run for 6 h on ice. All aminoacylation reactions were quenched with 3× volumes of 600 mM ammonium acetate (pH = 5) followed by ethanol precipitation of the aa-tRNA. Ethanol-precipitated aa-tRNAs were resuspended and stored in 10 mM potassium acetate (pH = 5) at –80 °C and were used without further purification (3).

To estimate aminoacylation efficiency, analytical-scale aminoacylation reactions were performed concurrently with and under the same conditions as the preparative aminoacylation reactions described above with the exception that [^{32}P] 3′-end–labeled tRNA was used in place of nonradiolabeled tRNA. [^{32}P] 3′-end–labeled tRNA was prepared by radiolabeling tRNA at the 3′ end with [^{32}P]-AMP using nucleotidyl transferase as previously described (3, 9) Nucleotidyl transferase was purified from an overexpressing plasmid that was a kind gift from Dr. Marcel Dupasquier and Prof. Ya-Ming Hou (both at Thomas Jefferson University, Philadelphia, PA). Labeling reactions were quenched with 3× volumes of 600 mM ammonium acetate (pH = 5), and aa-[^{32}P]-tRNAs were ethanol precipitated. Precipitated aa-[^{32}P]-tRNAs were resuspended in 10 mM potassium acetate (pH = 5) and digested with nuclease P1 (Sigma) for 10 min at room temperature (9). Subsequent separation of [^{32}P]-AMP and aa-[^{32}P]-AMP was achieved by TLC on polyethyleneimine-impregnated cellulose plates (EMD Chemicals, Inc.) using an acidic running buffer (100 mM ammonium chloride, 10% acetic acid) (9). TLC plates were exposed to a phosphorimaging screen (GE Healthcare Life Sciences) overnight and analyzed using a Storm 860 phosphor imager. The intensities of TLC spots corresponding to unreacted [^{32}P]-AMP ($I_{[32P]\text{-AMP}}$) and to aminoacylated product ($I_{aa\text{-}[32P]\text{-AMP}}$) were quantified using ImageQuant software. Aminoacylation efficiencies were calculated as $(I_{aa\text{-}[32P]\text{-AMP}})/(I_{[32P]\text{-AMP}} + I_{aa\text{-}[32P]\text{-AMP}}) \times 100$ (Fig. S1). These measured aminoacylation efficiencies were used to calculate the final concentrations of aa-tRNA in the peptide synthesis reactions.

The L-aa-tRNAs used to decode the third codon in the tripeptide and tetrapeptide synthesis reactions were aminoacylated with either the phenylalanyl- or lysyl-tRNA synthetases under conditions described elsewhere (2). Typical aminoacylation efficiencies were ∼35% for $tRNA^{Lys}$ and ∼95% for $tRNA^{Phe}$, as noted above.

Preparation of Tris-Polymix Buffer System for Peptide Synthesis Reactions. Peptide synthesis reactions were performed in a Tris-polymix buffer containing 50 mM Tris-acetate ($pH_{25\ °C}$ = 7.5), 100 mM potassium chloride, 5 mM ammonium acetate, 0.5 mM calcium acetate, 3.5 mM magnesium acetate, 6 mM 2-mercaptoethanol, 5 mM putrescine, and 1 mM spermidine (2, 4, 10).

Preparation of Ribosomal Initiation Complexes. Ribosomal initiation complexes were prepared in Tris-polymix buffer using slight modifications of a previously published in vitro initiation reaction protocol (2, 4, 10). For peptide synthesis reactions involving D/L-Phe-$tRNA^{Phe}$ and D/L-Val-$tRNA^{Val}$, the initiation reaction contained final concentrations of 1.1 μM tightly coupled 70S

ribosomes, 1.2 μM IF1, 1.5 μM IF2, 1.3 μM IF3, 1.1 mM GTP, 0.5 μM f-[^{35}S]-Met-tRNA^{fMet}, and 3.6 μM mRNA. For peptide synthesis reactions involving D/L-Lys-tRNA^{Lys}, the initiation reaction was identical to that used for the peptide synthesis reactions involving D/L-Phe-tRNA^{Phe} and D/L-Val-tRNA^{Val}, with the exception that the concentration of f-[^{35}S]-Met-tRNA^{fMet} was lowered to 0.12 μM.

IFs, 70S tightly coupled ribosomes, and GTP were incubated first for 10 min at 37 °C. mRNA was added next, followed by another incubation at 37 °C for 10 min. Finally, f-[^{35}S]-Met-tRNA^{fMet} was added. The mixture was incubated again at 37 °C for 10 min and was stored on ice until use. Ribosomal initiation complexes were used without further purification and were made fresh before each experiment.

T4gp32$_{1–20}$ mRNAs were used to form all ribosomal initiation complexes used in the peptide synthesis reactions. Ribosomal initiation complexes used for the synthesis of di- and tripeptides containing D/L-Phe were initiated using wild-type T4gp32$_{1–20}$. The second codon of this wild-type mRNA, which is UUU and encodes Phe, was mutated to GUU so as to encode Val, and the resulting mRNA, T4gp32$_{1–20}$(F2V), was used to prepare the ribosomal initiation complexes used in the synthesis of di- and tripeptides containing D/L-Val. Ribosomal initiation complexes used for the synthesis of di- and tripeptides containing D/L-Lys were prepared using a more extensively mutated T4gp32$_{1–20}$ mRNA [T4gp32$_{1–20}$(F2K/K3F/R4E/K5V/S6Y)]. Ribosomal initiation complexes used in the synthesis of tetrapeptides containing D/L-Phe were prepared using a similarly mutated T4gp32$_{1–20}$ mRNA [T4gp32$_{1–20}$(R4E/K5V/S6Y)].

Preparation of EF-Tu(GTP)aa-tRNA Ternary Complex Formation and EF-G Solutions. EF-Tu(GTP)aa-tRNA ternary complexes were prepared in a reaction containing final concentrations of 22.3 μM EF-Tu, 2.5 μM EF-Ts, 800 μM GTP, 2.2 μM aa-tRNA, 2.5 mM phosphoenol-pyruvate, and 0.001 units/μL pyruvate kinase in Tris-polymix buffer. EF-Tu, EF-Ts, and GTP were mixed first and incubated at 37 °C for 1 min and then cooled on ice for 1 min. aa-tRNA was then added and the mixture was incubated again for 1 min at 37 °C and stored on ice until use.

A separate mixture containing final concentrations of 21 μM EF-G, 1 mM GTP, 3 μM phosphoenol-pyruvate, and 0.001 units/μL pyruvate kinase in Tris-polymix buffer was prepared before use and stored on ice without incubation.

Peptide Synthesis Reactions Involving D/L-Phe-tRNA^{Phe} and D/L-Val-tRNA^{Val}. Before starting the peptide synthesis reactions, the EF-G solution described in *Preparation of EF-Tu(GTP)aa-tRNA Ternary Complex Formation and EF-G Solutions* was added to ribosomal initiation complexes that had been initiated using f-[^{35}S]-Met-tRNA^{fMet} as described in *Preparation of Ribosomal Initiation Complexes*. EF-Tu(GTP)aa-tRNA ternary complexes prepared as described in *Preparation of EF-Tu(GTP)aa-tRNA Ternary Complex Formation and EF-G Solutions* using ribozyme-aminoacylated D/L-aa-tRNA (as described in *Aminoacylation of tRNAs*) to decode the second codon of the mRNA and, when included, synthetase-aminoacylated L-aa-tRNA to decode the third or fourth codon of the mRNA were then added to the reaction mixture. The resulting peptide synthesis reactions were then incubated at 37 °C for the indicated time points. The final concentrations of reaction components were as follows: [ribosomal initiation complexes] = 0.5 μM; [f-(^{35}S)-Met-tRNA^{fMet}] = 0.25 μM; [mRNA] = 1.9 μM; [EF-Tu] = 10 μM; [D/L-aa-tRNA used to decode the second codon of the mRNA] = 1.0 μM; [L-aa-tRNA used to decode the third codon of the mRNA] = 1.0 μM; [L-aa-tRNA used to decode the fourth codon of the mRNA] = 1.0 μM; [EF-G] = 1.7 μM. Peptide synthesis reactions were quenched with potassium hydroxide to a final concentration of 160 mM. Around 0.5 μL of each quenched peptide synthesis reaction was spotted using a pipet onto cellulose TLC plates (EMD), and products were separated using eTLC in pyridine acetate buffer (5% pyridine, 20% acetic acid, pH = 2.8) (11). For all peptide synthesis reactions, eTLCs were run for 20 min at 1,200 V, with the exception of the fMet-D/L-Lys-Phe tripeptide synthesis reactions, which were run for 30 min at 1,200 V. eTLCs were then dried, exposed to a phosphorimaging screen overnight, and analyzed using a Storm 860 phosphor imager. The intensities of eTLC spots corresponding to unreacted f-[^{35}S]-Met (I_{fMet}) and to di-, tri-, and tetrapeptide products (I_{di}, I_{tri}, and I_{tetra}, respectively) were quantified using ImageQuant software. Percent f-[^{35}S]-Met converted to tripeptide was calculated as $(I_{tri})/(I_{fMet} + I_{di} + I_{tri}) \times 100$. Similarly, percent f-[^{35}S]-Met converted to dipeptide was calculated as $(I_{di})/(I_{fMet} + I_{di}) \times 100$. Percent f-[^{35}S]-Met converted to di- or tripeptide as a function of time was fit to a single exponential function of the form $y = A_1(e^{-x/\tau 1}) + y_0$ using Origin 7. The reciprocal of τ_1, measured in minutes, was divided by 60 to obtain k_{app} in units of s^{-1} (Table S1). Experiments were performed in duplicate, and the SE between measurements was reported.

Peptide Synthesis Reactions Involving D/L-Lys-tRNA^{Lys}. Peptide synthesis reactions involving D/L-Lys-tRNA^{Lys} were performed in a manner identical to that described in *Peptide Synthesis Reactions Involving D/L-Phe-tRNA^{Phe} and D/L-Val-tRNA^{Val}* with the exception that the final concentrations of several reaction components were slightly altered. These reaction components and their final concentrations were as follows: [ribosomal initiation complexes] = 0.12 μM; [f-(^{35}S)-Met-tRNA^{fMet}] = 0.06 μM; [EF-Tu] = 3.6 μM; [D/L-aa-tRNA used to decode the second codon of the mRNA] = 1 μM; [L-aa-tRNA used to decode the third codon of the mRNA] = 0.8 μM.

Primer Extension Inhibition, or Toeprinting, Reactions. The efficiency of the translocation step of the translation elongation cycle can be studied using a primer extension inhibition, or toeprinting, assay. Dipeptide synthesis reactions are carried out using an mRNA template that has been preannealed with a 5′-[^{32}P]–labeled DNA primer. Subsequent reverse transcription of the primer-annealed mRNA is strongly blocked when the reverse transcriptase encounters an mRNA-bound ribosome, consequently producing a 5′-[^{32}P]-labeled cDNA, or "toeprint," of a defined length that reports on the position of the ribosome on the mRNA. Analysis of the cDNA products by gel electrophoresis on a 9% sequencing polyacrylamide gel thus reports the position of the ribosome on the mRNA with single-nucleotide resolution.

To minimize the effects of intrinsically strong blocks of the reverse transcriptase that were detected in initial, control toeprinting reactions using the truncated T4gp32$_{1–20}$ mRNA variants and that likely originate from secondary structures in these mRNA variants, the full-length T4gp32$_{1–224}$ mRNA variants described in *Preparation of Ribosomal Initiation Complexes* were used in place of the truncated T4gp32$_{1–20}$ mRNA variants. For toeprinting reactions involving D/L-Phe-tRNA^{Phe}, the wild-type T4gp32$_{1–224}$ mRNA was used. For toeprinting reactions involving D/L-Val-tRNA^{Val}, the second codon of the wild-type T4gp32$_{1–224}$ mRNA, which is UUU and encodes Phe, was mutated to GUU so as to encode Val. For toeprinting reactions involving D/L-Lys-tRNA^{Lys}, the second codon of the wild-type T4gp32$_{1–224}$ mRNA was mutated from UUU to AAA so as to encode Lys, and the third codon of the wild-type T4gp32$_{1–224}$ mRNA, which is AAA and encodes Lys, was mutated to UUU so as to encode Phe. To ensure that the first 20 amino acids of this longer mRNA were identical to the first 20 amino acids of the shorter mRNA used in the peptide synthesis reactions involving D/L-Lys, the following mutations—R4E/K5V/S6Y—were also made.

The DNA primer used in the toeprinting reactions was radiolabeled with γ-[^{32}P]-ATP by preparing a reaction mixture containing 2.4 μM DNA primer (5′-TATTGCCATTCAGTTTAG-3′,

Integrated DNA Technologies), 1.4 μM γ-[^{32}P]-ATP (Perkin-Elmer), and 0.5 Units/μL T4 polynucleotide kinase (New England Biolabs) in 1× polynucleotide kinase buffer (New England Biolabs) and incubating it for 30 min at 37 °C. This was followed by incubation for 10 min at 75 °C to inactivate the T4 polynucleotide kinase and subsequent gel filtration through a G25 Sephadex spin column (GE Healthcare Life Sciences) to remove unincorporated γ-[^{32}P]-ATP. To anneal the ^{32}P-labeled DNA primer to each mRNA variant, a reaction mixture containing 5 μM of the mRNA variant and 0.25 μM ^{32}P-labeled DNA primer in 25 mM Tris-acetate ($pH_{25\ °C}$ = 7) was incubated for 90 s at 90 °C and slow cooled to room temperature by placing the reaction mixture on the benchtop.

Dipeptide synthesis reactions used for toeprinting were carried out under conditions identical to those described above in *Peptide Synthesis Reactions Involving D/L-Phe-tRNA^{Phe} and D/L-Val-tRNA^{Val}* and *Peptide Synthesis Reactions Involving D/L-Lys-tRNA^{Lys}* with three exceptions. First, fMet-tRNA^{fMet} was added to a final concentration of 0.5 μM. Second, T4gp32$_{1–224}$ mRNA (A) was used at a final concentration of 0.25 μM for dipeptide reactions involving D/L-Phe-tRNA^{Phe} and D/L-Val-tRNA^{Val} and a final concentration of 0.06 μM for dipeptide reactions involving D/L-Lys-tRNA^{Lys} (in all cases, mRNA was the limiting reagent in the preparation of ribosomal initiation complexes) and (B) was preannealed to a γ-[^{32}P]-ATP–labeled DNA primer targeting the 3′ end of the mRNAs. Thus, the concentration of fully initiated ribosomal complexes used in peptide synthesis reactions for toeprinting was the same as in the peptide synthesis reactions described in *Peptide Synthesis Reactions Involving D/L-Phe-tRNA^{Phe} and D/L-Val-tRNA^{Val}* and *Peptide Synthesis Reactions Involving D/L-Lys-tRNA^{Lys}* with only the limiting reagent being changed. Third, dipeptide synthesis reactions were quenched with 4× reaction volumes of toeprinting mix (1.25 mM viomycin; 625 μM each dGTP, dCTP, and dTTP; and 2.2 mM dATP in 1.25– Tris-polymix buffer, 12.5 mM magnesium acetate), with the antibiotic viomycin included because it strongly inhibits EF-G–catalyzed translocation (12).

Following the dipeptide synthesis reaction and quenching with toeprinting mix, mRNAs were then reverse-transcribed by adding avian myeloblastosis virus (AMV) reverse transcriptase (Promega) to a final concentration of 0.6 Units/μL and incubated for 15 min at 37 °C. The 5′-[^{32}P]–labeled cDNA reverse transcription products were phenol extracted twice, chloroform extracted twice, and then ethanol precipitated. The resulting pellets were resuspended in gel loading buffer (23 M formamide, 0.09% bromophenol blue, and 0.09% xylene cyanol) and separated using gel electrophoresis on a 9% denaturing polyacrylamide gel. Gels were dried and imaged by phosphorimaging.

Phosphorimages of the gels were analyzed using ImageQuant software to quantify the intensities of the bands corresponding to cDNAs produced by stops of the reverse transcriptase at the +15, +16, +18, and +19 mRNA nucleotide positions (where the positive numerical values indicate the mRNA nucleotide position downstream from and relative to the adenosine nucleotide of the AUG start codon). Control toeprinting reactions in which ribosomes had been omitted from the dipeptide synthesis reactions were performed. cDNA products from these control toeprinting reactions were loaded in the "control" lane of each gel; the bands in these control lanes report on the intrinsic stop sites of the reverse transcriptase along each mRNA. A high-intensity band corresponding to the +15 mRNA nucleotide position reports on the presence of a properly positioned ribosomal initiation complex on the mRNA (I_{+15}). In the fMet-tRNA^{fMet} lane, ribosomal initiation complexes prepared as described in *Preparation of Ribosomal Initiation Complexes*, with the exception that radiolabeled, primer-annealed mRNA was used in place of the mRNA, yielded a high I_{+15}. Addition of an EF-Tu(GTP) D/L-aa-tRNA ternary complex to the ribosomal initiation complex, however, results in a decrease in I_{+15} and a corresponding increase in the intensity of the band corresponding to the 16 mRNA nucleotide position (I_{+16}); subsequent addition of EF-G then results in a decrease in I_{+16} and corresponding increases in the intensities of the bands corresponding to the 18 and 19 mRNA nucleotide positions (I_{+18} and I_{+19}). For toeprinting reactions involving D/L-Phe-tRNA^{Phe} or D/L-Val-tRNA^{Val}, percent translocation was calculated as $[(I_{+18} + I_{+19})/(I_{+15} + I_{+16} + I_{+18} + I_{+19})] \times 100$. The ability of the ribosome to move three nucleotides, or one codon, along the mRNA from the +15 to the +18 position demonstrates one round of translocation.

For toeprinting reactions involving D/L-Lys-tRNA^{Lys}, I_{+15} was corrected due to greater intensity in the control lane than was detected in the control lanes of the toeprinting reactions involving D/L-Phe-tRNA^{Phe} and D/L-Val-tRNA^{Val}. I_{+15}* was generated in the following way: From the control lane, $[(I_{+15})/(I_{\text{full-length mRNA band}})]$ was determined. The total intensity of the full-length mRNA band in the fMet-tRNA^{fMet} lane was then multiplied by this fraction, and this product was subtracted from the I_{+15} in the fMet-tRNA^{fMet} experiment to generate a final, corrected intensity value for the I_{+15} in the fMet-tRNA^{fMet} experiment. Likewise, it was also necessary to correct the values of I_{+16}, I_{+18}, and I_{+19} in the same way to generate I_{+16}*, I_{+18}*, and I_{+19}*. In addition, because of the propensity for Lys-tRNA^{Lys} to miscode (13), it was necessary to consider the intensities of the bands corresponding to the +21 and +22 mRNA nucleotide positions, both of which were corrected as described above to generate I_{+21}* and I_{+22}*. Percent translocation using the corrected intensities was then calculated as $[(I_{+18}^* + I_{+19}^* + I_{+21}^* + I_{+22}^*)/(I_{+15}^* + I_{+16}^* + I_{+18}^* + I_{+19}^* + I_{+21}^* + I_{+22}^*)] \times 100$.

Percent translocation as a function of time obtained from analysis of the phosphorimages of the gels was fit to a single exponential function of the form $y = A_1(e^{-x/\tau 1}) + y_0$ using Origin 7. The reciprocal of τ_1, measured in minutes, was divided by 60 to obtain k_{app} in units of s^{-1}. Experiments were performed in duplicate, and the SE between measurements is reported.

Nitrocellulose Filter Binding Experiments. Dipeptide synthesis reactions were carried out under conditions identical to those described in *Peptide Synthesis Reactions Involving D/L-Phe-tRNA^{Phe} and D/L-Val-tRNA^{Val}* and *Peptide Synthesis Reactions Involving D/L-Lys-tRNA^{Lys}*. A 0.5-μL aliquot of each ribosomal initiation complex was removed before addition of the EF-Tu(GTP)D/L-aa-tRNA ternary complex to represent the 0 time point. Following addition of the EF-Tu(GTP)D/L-aa-tRNA ternary complex to the ribosomal initiation complex, a 0.5-μL aliquot of the resulting dipeptide synthesis reaction was removed at each of the indicated time points. These 0.5-μL aliquots were diluted by the addition of 49.5 μL stop buffer [50 mM Tris·hydrochloride ($pH_{25\ °C}$ = 7.5), 1 M ammonium chloride, 15 mM magnesium acetate]. For each time point, 10 μL of this mixture was pipetted onto a nitrocellulose filter that was not exposed to vacuum, and 30 μL of this mixture was pipetted onto a nitrocellulose filter that had been placed over the wells of a vacuum manifold (Millipore) and that had been prewetted with chilled stop buffer. Filters on the manifold were then extensively washed with stop buffer. A flow rate of ∼5 mL/min was maintained through the nitrocellulose filters. Scintillation counting was subsequently used to obtain the counts on the nitrocellulose filters that had and had not been exposed to vacuum at each time point, and differences in the amount pipetted onto each filter were taken into account. The percent f-[^{35}S]-Met retained on nitrocellulose filters was calculated by dividing the normalized counts of the filters that had been exposed to vacuum by those filters that had not been exposed to vacuum at each time point and multiplying by 100. Percent f-[^{35}S]-Met retained on nitrocellulose filters as a function of time was fit to a single exponential function of the form $y = A_1(e^{-x/\tau 1}) + y_0$. The reciprocal of

τ_1, measured in minutes, was divided by 60 to obtain k_{app} in units of s^{-1}. Experiments were performed at least three times and the SD between measurements is reported.

Pmn Reactions. Dipeptide synthesis reactions were performed as described in *Peptide Synthesis Reactions Involving D/L-Phe-tRNA^{Phe} and D/L-Val-tRNA^{Val}* and *Peptide Synthesis Reactions Involving D/L-Lys-tRNA^{Lys}*. The resulting dipeptide synthesis reactions were incubated for up to 10 min (~2.5 min for the syntheses of fMet-L-Phe, fMet-L-Lys, and fMet-L-Val dipeptides; ~5 min for the synthesis of fMet-D-Lys dipeptide; and ~10 min for the syntheses of fMet-D-Phe and fMet-D-Val dipeptides) such that the dipeptide synthesis reactions went to completion and the resulting dipeptidyl-tRNAs were fully translocated into the ribosomal peptidyl-tRNA binding (P) site. Pmn in Tris-polymix buffer was then added to the dipeptide synthesis reactions to a final concentration of 24 mM, and the Pmn reactions were allowed to proceed at 37 °C until the indicated time points. The Pmn reactions were quenched, the reaction products were separated, and the results were analyzed as described in *Peptide Synthesis Reactions Involving D/L-Phe-tRNA^{Phe} and D/L-Val-tRNA^{Val}*. Percent f-[^{35}S]-Met converted to dipeptide-Pmn was quantified as $(I_{di\text{-}pmn})/(I_{fMet} + I_{di} + I_{di\text{-}pmn}) \times 100$. Percent f-[^{35}S]-Met converted to dipeptide-Pmn as a function of time was then fit to a single exponential function of the form $y = A_1(e^{-x/\tau 1}) + y_0$. The reciprocal of τ_1, measured in minutes, was divided by 60 to obtain k_{app} in units of s^{-1}. Experiments were performed in duplicate, and the SE between measurements is reported.

Chemical Probing Experiments. Dipeptide synthesis reactions to produce ECs carrying either fMet-L-Phe-tRNA^{Phe} or fMet-D-Phe-tRNA^{Phe} at the P site were prepared as described in *Peptide Synthesis Reactions Involving D/L-Phe-tRNA^{Phe} and D/L-Val-tRNA^{Val}*, with the exception that the final concentration of fMet-tRNA^{fMet} was adjusted to 0.75 μM to ensure that 70S ribosomes were the limiting reagent. Dipeptide synthesis reactions involving L-Phe-tRNA^{Phe} and D-Phe-tRNA^{Phe} were allowed to proceed for 2.5 min and 10 min, respectively. These dipeptide synthesis reaction times ensured that the dipeptide synthesis reactions had gone to completion, and the resulting dipeptidyl-tRNAs had been fully translocated into the P site. Control reactions containing vacant ribosomes (i.e., not carrying any tRNAs) rather than ECs were prepared identically to that described in *Peptide Synthesis Reactions Involving D/L-Phe-tRNA^{Phe} and D/L-Val-tRNA^{Val}*, with the exception that acylated tRNAs were omitted.

Following the incubation times listed in the previous paragraph, DMS chemical probing reactions were performed using slight modifications of a previously published protocol (14). DMS was diluted 10-fold with DMS buffer (80% ethanol in Tris-polymix buffer) immediately before use. DMS modification of ECs was initiated by adding 1 μL of the diluted DMS solution to the ECs. Upon addition of DMS, the ECs were immediately placed on ice and incubated for 45 min. Four DMS chemical probing reactions were performed during each experiment: (*i*) ECs containing fMet-L-Phe-tRNA^{Phe} in the P site were treated with DMS buffer lacking DMS, (*ii*) vacant ribosomes were treated with DMS, (*iii*) ECs containing fMet-L-Phe-tRNA^{Phe} were treated with DMS, and (*iv*) ECs containing fMet-D-Phe-tRNA^{Phe} were treated with DMS. We added 25 ng of glycogen (Ambion) to all reactions immediately before precipitating the rRNA with 95% ethanol. Following ethanol precipitation, pellets containing the precipitated rRNA were dissolved in 200 μL of a solution consisting of 0.3 M NaOAc, 2.5 mM EDTA, and 0.5% SDS. The resulting solution was extracted with phenol three times with vigorous agitation for 5 min followed by chloroform extraction two times with vigorous agitation for 3 min. Following the phenol and chloroform extractions, the rRNA was ethanol precipitated a second time. The resulting pellets were dissolved in 15 μL NanoPure H_2O.

A 17-nucleotide DNA primer complementary to 23S rRNA in the region of A2058 and A2059 in the PTC and named for the first 23S rRNA nucleotide that is reverse-transcribed (primer 2117, 5′-CAAAGCCTCCCACCTAT-3′) was radiolabeled as described in *Primer Extension Inhibition, or Toeprinting, Reactions*. Additional 17-nucleotide DNA primers complementary to 23S rRNA that were tested, but that did not reveal reactivity differences in the presence of a P-site peptidyl-D-aa-tRNA, included primers 2639, 2493, and 800, which probe the regions surrounding 23S rRNA nucleotides A2602, A2451, and A751, respectively, in the PTC. To anneal the ^{32}P-labeled DNA primer to the 23S rRNA, a reaction mixture containing ~1.0 pmol rRNA and 0.7 pmol [^{32}P]-labeled DNA primer in sequencing buffer [25 mM Tris•HCl ($pH_{25\ °C}$ = 8.3), 40 mM KCl, and 5 mM $MgCl_2$] was incubated for 5 min at 65 °C (final volume = 10 μL) and then slow cooled to room temperature on the benchtop. A mixture of deoxynucleotides at a final concentration of 500 μM of each deoxynucleotide in sequencing buffer and 18 units of AMV reverse transcriptase were then added to the primer-annealed 23S rRNA samples, and the resulting primer extension reactions (final volume = 20 μL) were incubated at 42 °C for 30 min. Sequencing reactions were performed using rRNA that was isolated from unmodified vacant ribosomes in a manner that was identical to that isolated from ECs and were run in a manner identical to that for the primer extension reactions with the exception that 25 μM of specific dideoxynucleotides were included in the mixture of deoxynucleotides. Primer extension and sequencing reactions were quenched with an equal reaction volume of gel loading buffer (23 M formamide, 0.09% bromophenol blue, and 0.09% xylene cyanol), and the cDNA products were separated using gel electrophoresis on a 7% denaturing polyacrylamide gel.

Gels were scanned and visualized by phosphorimaging, and the resulting band intensities, which correspond to the average reactivity of each nucleotide with the chemical probe, were quantified and analyzed using the semi-automated footprinting analysis (SAFA) software program (15). To normalize the fMet-L-Phe-tRNA^{Phe} and fMet-D-Phe-tRNA^{Phe} lanes to account for small, potential differences in the total amount of radiolabeled cDNA that was loaded into each lane, we implemented a previously published approach using an algorithm that is built into SAFA (16).

Briefly, for each experiment, the algorithm compares the intensity of each band in the fMet-L-Phe-tRNA^{Phe} lane with the intensity of the corresponding band in the fMet-D-Phe-tRNA^{Phe} lane and identifies those bands that exhibit the smallest variations in intensity between the fMet-L-Phe-tRNA^{Phe} lane and fMet-D-Phe-tRNA^{Phe} lane (i.e., the invariant bands). Subsequently, for the set of invariant bands in each lane, the algorithm identifies those bands that are most tightly clustered around the median intensity of the set of invariant bands (i.e., such that high-intensity invariant bands occurring as a result of the reverse transcriptase encountering sequences at which it has a strong natural tendency to stop and low-intensity invariant bands that are too noisy to be confidently analyzed are excluded from the analysis) and ranks them in order by increasing dispersion from the median value. The intensities of the top-ranked invariant bands therefore (*i*) primarily reflect the chemical modification of the corresponding residues (as opposed to reflecting natural stops of the reverse transcriptase); (*ii*) are well above the noise such that they can be confidently analyzed; (*iii*) vary the least between the fMet-L-Phe-tRNA^{Phe} and fMet-D-Phe-tRNA^{Phe} lanes; and (*iv*) are the most similar to each other. Thus, small differences between the intensity of each top-ranked invariant band in the fMet-L-Phe-tRNA^{Phe} lane and its corresponding band in the fMet-D-Phe-tRNA^{Phe} lane primarily reflect small differences in the total amount of radiolabeled cDNA that was loaded into each lane of the gel.

The raw intensity of each band in each lane was then divided by the average intensity of the five top-ranked invariant bands in that

lane to normalize the band intensities for small differences in the total amount of radiolabeled cDNA that was loaded into each lane of the gel. The fMet-D-Phe-tRNA^{Phe} lane was then set as the reference lane, and the normalized band intensities from the fMet-D-Phe-tRNA^{Phe} lane were divided by the corresponding normalized band intensities from the same fMet-D-Phe-tRNA^{Phe} lane, resulting in the calculation of a D/D ratio for each nucleotide that is equal to 1 and that serves as a reference. Subsequently, the normalized band intensities from the fMet-L-Phe-tRNA^{Phe} lane were divided by the corresponding normalized band intensities from the fMet-D-Phe-tRNA^{Phe} lane, resulting in the calculation of an L/D value for each nucleotide that reflects the difference in the DMS reactivity of that nucleotide in an EC carrying a P-site fMet-L-Phe-tRNA^{Phe} relative to an EC carrying a P-site fMet-D-Phe-tRNA^{Phe}. The D/D ratio for each nucleotide (denoted by the black line connecting the filled black circles denoted as "D/D Reference" in Fig. S7*B*) and the mean and SD of the L/D value for each nucleotide (denoted by the gray bars and corresponding black error bars labeled as "Mean L/D" in Fig. S7*B*) were calculated from the three independent chemical probing experiments.

To determine the significance of changes in the L/D value of each nucleotide, we compared the L/D value of each nucleotide to the average L/D ratio of all gel nucleotides (denoted as the red line labeled "Average L/D" in Fig. S7*B*) and to the 1 and 2 SD uncertainty estimates (denoted by the red and orange dashed lines labeled "±1 SD From the Average L/D" and "±2 SD From the Average L/D," respectively). A nucleotide that exhibits an L/D value that is above or below the average L/D is a nucleotide whose DMS reactivity is altered in an EC carrying a P-site fMet-L-Phe-tRNA^{Phe} relative to an EC carrying a P-site fMet-D-Phe-tRNA^{Phe}.

Molecular Modeling and Computer Simulations. The starting models of the MD simulations in the current study were prepared by using empirically determined structures of the ribosome as constraints. Specifically, we used the coordinates of the PTC from a high-quality and high-resolution X-ray crystallographic structure that was empirically determined by the Ramakrishnan group of a ribosome carrying Phe-tRNA^{Phe}s at the P site and the ribosomal aa-tRNA binding (A) site in which the ester linkages between the phenylalanines and the A76s of the tRNAs had been modified to amide linkages (17) as constraints for our simulations. To prepare structural models for our simulations, however, we used Phe-tRNA^{Phe}s containing ester linkages between the phenylalanines and the A76s of the tRNAs and used only the coordinates of backbone atoms of the Phe-tRNA^{Phe} as constraints, ignoring the slight differences in the atom types. Likewise, the MD simulations were performed using well-established MD algorithms to simulate the dynamics of the ribosome. Specifically, we used parameters from the assisted model building and energy refinement (AMBER) force field using the ff99SB parameter set (AMBER99SB) (18, 19) to perform the MD simulations. These MD simulation methods and the AMBER99SB force field have been validated over many years to be reliable for describing the molecular interactions of protein–RNA complexes, such as the ribosome (20).

The modeling of our simulation systems started with a fully solvated *E. coli* ribosome model developed by Trabuco et al. (21) that carries tRNAs at the P and A sites and a vacant ribosomal tRNA exit (E) site. To construct the EC carrying fMet-L-Phe-tRNA^{Phe} at the P site and Lys-tRNA^{Lys} at the A site, the P- and A-site tRNAs in Trabuco's ribosome model were replaced with a P-site fMet-L-Phe-tRNA^{Phe} and an A-site Lys-tRNA^{Lys} that were modeled based on sequence information in the tRNAdb database (22). The backbone coordinates for the acylated P- and A-site tRNAs in our models were assigned using the coordinates of the corresponding atoms in the previously deposited crystallographic structure from Protein Data Bank (PDB) ID code 2WDK (17). The EC model was then equilibrated for 30 ns by performing an equilibrium MD simulation with distance restraints between the two tRNAs and adjacent ribosome nucleotides based on crystallographic structures from PDB ID codes 2WDK–2WDL (17) to ensure proper interactions between the acceptor stems of the tRNAs and the ribosome (23).

To achieve enough sampling at an acceptable computational cost, we constructed a reduced model of the EC by including only residues within 60 Å of the peptidyl-transferase center core, as defined by 23S rRNA nucleotides 2585, 2451, 2062, 2063, 2505, and 2506 and the acceptor stems of the P- and A-site tRNAs. Atoms more than 60 Å away from the PTC core were immobilized and not included in the MD simulations. The water box including ions in solution for the reduced model were modeled using a previously described protocol (21), resulting in a system size of ~320,000 atoms for the actual (i.e., unconstrained) MD simulations.

To obtain a model of an EC carrying an fMet-D-Phe-tRNA^{Phe} at the P site, we used the Visual Molecular Dynamics (VMD) (24) plugin "chirality" (25) to invert the stereochemistry of the alpha carbon of the L-Phe in the model of an EC carrying an fMet-L-Phe-tRNA^{Phe} at the P site that was described above. During the first 5-ns equilibrium MD simulation of the EC carrying fMet-D-Phe-tRNA^{Phe} in the P site, the fMet-D-Phe dipeptidyl moiety quickly adopted a unique orientation that was significantly different from that adopted by the fMet-L-Phe moiety during the first 5-ns equilibrium MD simulation of the EC carrying an fMet-L-Phe-tRNA^{Phe} at the P site. This unique orientation of the fMet-D-Phe moiety was maintained throughout the subsequent simulations. To test whether the unique orientation of the fMet-D-Phe dipeptidyl moiety might have been caused by the specific initial condition of the EC that was used in the simulation, three independent accelerated MD (aMD) simulations (26, 27) with dihedral potential boost were performed for the EC carrying an fMet-D-Phe-tRNA^{Phe}. All three aMD simulations, each of which was 30 ns long, resulted in a converged conformation of the fMet-D-Phe dipeptidyl moiety within the PTC core that was identical to that observed in our equilibrium MD simulations. The aMD simulations, which boost sampling of normal equilibrium MD simulations, were only used to test whether there were other favored conformations of the fMet-D-Phe dipeptidyl moiety within the PTC core; the results of the normal equilibrium MD simulation were used for all other analyses.

All simulations were performed using the Nanoscale Molecular Dynamics version 2.9 (NAMD 2.9) program (28) with the AMBER99SB force field (18, 19), which includes parameters for modified nucleosides (29). Modeling and analysis also used the program VMD (24). The equations of motion were integrated with a 2-fs time step, and bonded interactions, nonbonded short-range interactions, and nonbonded long-range interactions were calculated every 2 fs, 4 fs, and 6 fs, respectively. We performed two 100-ns-long equilibrium MD simulations for each of the ECs carrying either an fMet-L-Phe-tRNA^{Phe} or an fMet-D-Phe-tRNA^{Phe} at the P site. MD simulation trajectories were saved with a frame rate of 5 ps. The last 30-ns data of each simulation trajectory were used for all analyses [for example, for generating average structures by running the VMD (24) command "measure avpos" with the relevant trajectory].

1. Powers T, Noller HF (1991) A functional pseudoknot in 16S ribosomal RNA. *EMBO J* 10(8):2203–2214.
2. Fei J, et al. (2010) A highly purified, fluorescently labeled in vitro translation system for single-molecule studies of protein synthesis. *Methods Enzymol* 472:221–259.
3. Effraim PR, et al. (2009) Natural amino acids do not require their native tRNAs for efficient selection by the ribosome. *Nat Chem Biol* 5(12):947–953.
4. Blanchard SC, Kim HD, Gonzalez RL, Jr, Puglisi JD, Chu S (2004) tRNA dynamics on the ribosome during translation. *Proc Natl Acad Sci USA* 101(35):12893–12898.

5. Datta D, Wang P, Carrico IS, Mayo SL, Tirrell DA (2002) A designed phenylalanyl-tRNA synthetase variant allows efficient in vivo incorporation of aryl ketone functionality into proteins. *J Am Chem Soc* 124(20):5652–5653.
6. Shimizu Y, et al. (2001) Cell-free translation reconstituted with purified components. *Nat Biotechnol* 19(8):751–755.
7. Sarin PS, Zamecnik PC (1964) On the stability of aminoacyl-s-RNA to nucleophilic catalysis. *Biochim Biophys Acta* 91:653–655.
8. Murakami H, Ohta A, Ashigai H, Suga H (2006) A highly flexible tRNA acylation method for non-natural polypeptide synthesis. *Nat Methods* 3(5):357–359.
9. Ledoux S, Uhlenbeck OC (2008) [3′-32P]-labeling tRNA with nucleotidyltransferase for assaying aminoacylation and peptide bond formation. *Methods* 44(2):74–80.
10. Pavlov MY, Ehrenberg M (1996) Rate of translation of natural mRNAs in an optimized in vitro system. *Arch Biochem Biophys* 328(1):9–16.
11. Weinger JS, Parnell KM, Dorner S, Green R, Strobel SA (2004) Substrate-assisted catalysis of peptide bond formation by the ribosome. *Nat Struct Mol Biol* 11(11): 1101–1106.
12. Joseph S, Noller HF (1998) EF-G-catalyzed translocation of anticodon stem-loop analogs of transfer RNA in the ribosome. *EMBO J* 17(12):3478–3483.
13. Zaher HS, Green R (2009) Quality control by the ribosome following peptide bond formation. *Nature* 457(7226):161–166.
14. Stern S, Moazed D, Noller HF (1988) Structural analysis of RNA using chemical and enzymatic probing monitored by primer extension. *Methods Enzymol* 164: 481–489.
15. Das R, Laederach A, Pearlman SM, Herschlag D, Altman RB (2005) SAFA: Semi-automated footprinting analysis software for high-throughput quantification of nucleic acid footprinting experiments. *RNA* 11(3):344–354.
16. Takamoto K, He Q, Morris S, Chance MR, Brenowitz M (2002) Monovalent cations mediate formation of native tertiary structure of the Tetrahymena thermophila ribozyme. *Nat Struct Biol* 9(12):928–933.
17. Voorhees RM, Weixlbaumer A, Loakes D, Kelley AC, Ramakrishnan V (2009) Insights into substrate stabilization from snapshots of the peptidyl transferase center of the intact 70S ribosome. *Nat Struct Mol Biol* 16(5):528–533.
18. Cornell WD, et al. (1995) A second generation force field for the simulation of proteins, nucleic acids, and organic molecules. *J Am Chem Soc* 117:5179–5197.
19. Hornak V, et al. (2006) Comparison of multiple Amber force fields and development of improved protein backbone parameters. *Proteins* 65(3):712–725.
20. Mackerell AD, Jr, Nilsson L (2008) Molecular dynamics simulations of nucleic acid-protein complexes. *Curr Opin Struct Biol* 18(2):194–199.
21. Trabuco LG, et al. (2010) The role of L1 stalk-tRNA interaction in the ribosome elongation cycle. *J Mol Biol* 402(4):741–760.
22. Jühling F, et al. (2009) tRNAdb 2009: Compilation of tRNA sequences and tRNA genes. *Nucleic Acids Res* 37(Database issue):D159–D162.
23. Nissen P, Ippolito JA, Ban N, Moore PB, Steitz TA (2001) RNA tertiary interactions in the large ribosomal subunit: The A-minor motif. *Proc Natl Acad Sci USA* 98(9): 4899–4903.
24. Humphrey W, Dalke A, Schulten K (1996) VMD: Visual Molecular Dynamics. *J Mol Graph* 14(1):33–38, 27–28.
25. Schreiner E, Trabuco LG, Freddolino PL, Schulten K (2011) Stereochemical errors and their implications for molecular dynamics simulations. *BMC Bioinformatics* 12:190.
26. Hamelberg D, Mongan J, McCammon JA (2004) Accelerated molecular dynamics: A promising and efficient simulation method for biomolecules. *J Chem Phys* 120(24): 11919–11929.
27. Wang Y, Harrison CB, Schulten K, McCammon JA (2011) Implementation of accelerated molecular dynamics in NAMD. *Comput Sci Discov* 4(1):015002.
28. Phillips JC, et al. (2005) Scalable molecular dynamics with NAMD. *J Comput Chem* 26(16):1781–1802.
29. Aduri R, et al. (2007) AMBER force field parameters for the naturally occurring modified nucleosides in RNA. *J Chem Theory Comput* 3(4):1464–1475.

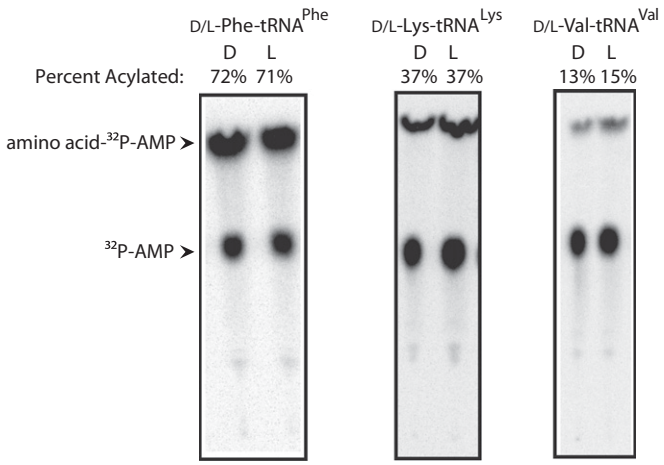

Fig. S1. TLC analysis of aminoacylation efficiency. The efficiency with which tRNA^{Phe}, tRNA^{Lys}, and tRNA^{Val} could be aminoacylated using the eFx or dFx ribozymes was analyzed by TLC as described in *Aminoacylation of tRNAs*. The calculated aminoacylation efficiencies are indicated at the top of each lane of each TLC.

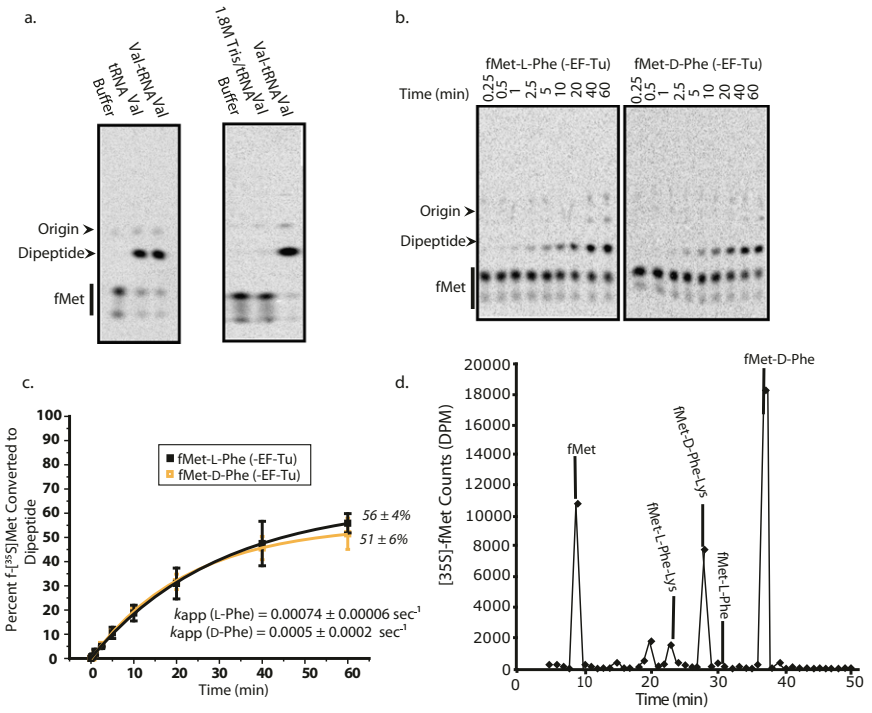

Fig. S2. Analysis of $tRNA^{Val}$ before experimental use, of the EF-Tu dependence of dipeptide synthesis, and of ribosome-synthesized peptide products. (*A*) $tRNA^{Val}$ obtained from commercial sources had to be deacylated before use in aminoacylation reactions and peptide synthesis reactions. (*A*, *Left*) Buffer (Buffer lane), $tRNA^{Val}$ obtained commercially from Sigma ($tRNA^{Val}$ lane), and Val-$tRNA^{Val}$ prepared by aminoacylating $tRNA^{Val}$ obtained commercially from Sigma (Val-$tRNA^{Val}$ lane) were used to form EF-Tu(GTP)aa-tRNA ternary complexes as described in *Preparation of EF-Tu(GTP)aa-tRNA Ternary Complex Formation and EF-G Solutions* and in dipeptide synthesis reactions as described in *Peptide Synthesis Reactions Involving D/L-Phe-*$tRNA^{Phe}$ *and D/L-Val-*$tRNA^{Val}$. The appearance of an eTLC spot corresponding to the fMet-L-Val dipeptide in the $tRNA^{Val}$ lane demonstrates that a portion of the $tRNA^{Val}$ obtained commercially from Sigma was acylated. (*A*, *Right*) Buffer (Buffer lane), $tRNA^{Val}$ obtained commercially from Sigma and treated with 1.8 M Tris·hydrochloride ($pH_{25\ °C} = 8$) for 3 h at 37 °C (1) (1.8 M Tris/$tRNA^{Val}$ lane), and Val-$tRNA^{Val}$ prepared by aminoacylating $tRNA^{Val}$ obtained commercially from Sigma (Val-$tRNA^{Val}$ lane) were used to form EF-Tu(GTP)aa-tRNA ternary complexes as described in *Preparation of EF-Tu(GTP)aa-tRNA Ternary Complex Formation and EF-G Solutions* and used in dipeptide synthesis reactions as described in *Peptide Synthesis Reactions Involving D/L-Phe-*$tRNA^{Phe}$ *and D/L-Val-*$tRNA^{Val}$. The absence of an eTLC spot corresponding to the fMet-L-Val dipeptide in the 1.8 M Tris/$tRNA^{Val}$ lane demonstrates that the treatment with 1.8 M Tris efficiently deacylated the $tRNA^{Val}$ obtained commercially from Sigma. Similar control dipeptide synthesis reactions using $tRNA^{Phe}$ and $tRNA^{Lys}$ obtained commercially from Sigma demonstrated that these two tRNAs were not acylated before aminoacylation using the ribozyme. (*B*) eTLC analysis of f-[^{35}S]-Met-L-Phe and f-[^{35}S]-Met-D-Phe dipeptide synthesis reaction time courses performed in the absence of EF-Tu. (*C*) A plot of the percent f-[^{35}S]-Met converted to dipeptide obtained from the eTLC shown in *B* as a function of time reveals that the rates of f-[^{35}S]-Met-L-Phe and f-[^{35}S]-Met-D-Phe synthesis in the absence of EF-Tu are very similar. In addition, the rate of f-[^{35}S]-Met-D-Phe dipeptide synthesis in the absence of EF-Tu shown here is 40-fold slower than the rate of f-[^{35}S]-Met-D-Phe synthesis in the presence of EF-Tu (shown in Fig. 1). Each experiment was performed in duplicate. These controls demonstrate that D-aa-tRNAs are delivered to ribosomal initiation complexes in an EF-Tu–dependent manner. (*D*) Reverse-phase HPLC of L- or D-amino acid–containing peptides synthesized by the ribosome and chemically synthesized, L- or D-amino acid–containing di- and tripeptides confirmed that D-amino acids were indeed incorporated into ribosome-synthesized peptides. The HPLC chromatogram consists of unincorporated f-[^{35}S]-Met as well as f-[^{35}S]-Met–labeled peptides synthesized by the ribosome in the tripeptide synthesis reaction of f-[^{35}S]-Met-D-Phe-Lys. The elution positions of authentic fMet, fMet-L-Phe, fMet-D-Phe, fMet-L-Phe-Lys, and fMet-D-Phe-Lys markers, in which the peptides were prepared by solid-phase peptide synthesis, were monitored by their UV-Vis absorbance at 190 nm, and are indicated by black bars above the peaks in the HPLC chromatogram. The unreacted f-[^{35}S]-Met amino acid and peptides synthesized by the ribosome in tripeptide synthesis reactions were coinjected with authentic fMet amino acid and chemically synthesized, L- and D-amino acid–containing di- and tripeptide markers onto a C18 column (Waters–X bridge) and the gradient used to separate the various peptide products was 10% MeCN to 12% MeCN over 12 min, isocratic 20% MeCN from 12 to 15 min, and 20% MeCN to 35% MeCN from 15 to 58 min.

1. Sarin PS, Zamecnik PC (1964) On the stability of aminoacyl-s-RNA to nucleophilic catalysis. *Biochim Biophys Acta* 91:653–655.

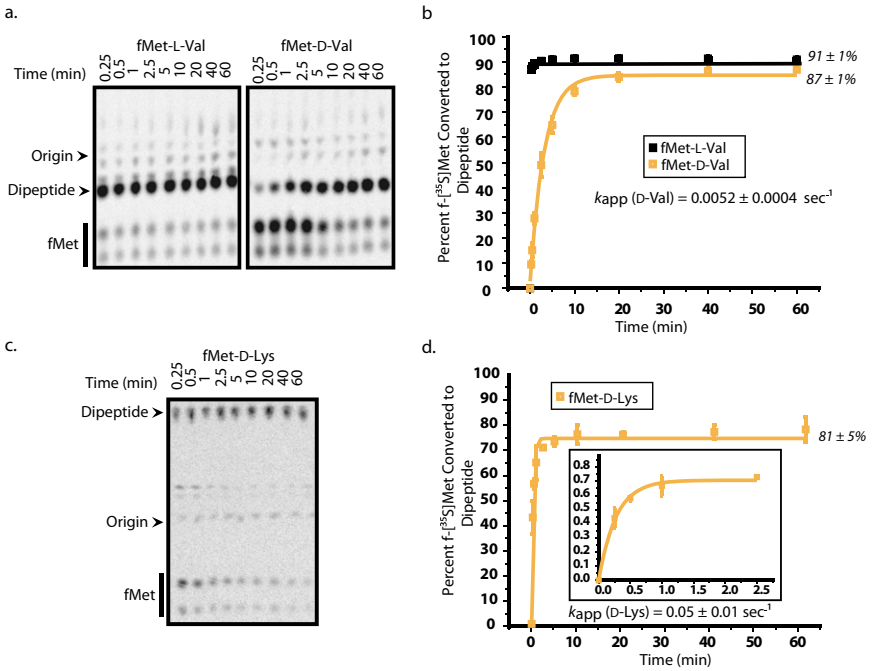

Fig. S3. Dipeptide synthesis reactions involving D-Val-tRNA^{Val} and D-Lys-tRNA^{Lys} go to completion. eTLC analysis of (*A*) f-[^{35}S]-Met-D/L-Val and (*C*) f-[^{35}S]-Met-D-Lys dipeptide synthesis reactions. Plots of percent f-[^{35}S]-Met converted to dipeptide as a function of time for dipeptide synthesis reactions involving (*B*) D-Val-tRNA^{Val} and (*D*) D-Lys-tRNA^{Lys}. These experiments demonstrate that dipeptide synthesis reactions involving D-Val-tRNA^{Val} and D-Lys-tRNA^{Lys} go to completion, with 87% or 81% of f-[^{35}S]-Met-tRNA^{fMet} converted to dipeptide, respectively. Experiments were run in duplicate, and the SE is reported. The fMet-L-Lys dipeptide synthesis reaction as a function of time was not performed because the f-[^{35}S]-Met-L-Lys-Phe tripeptide synthesis reaction was already complete at the 15-s time point (Fig. S4 *C* and *D*).

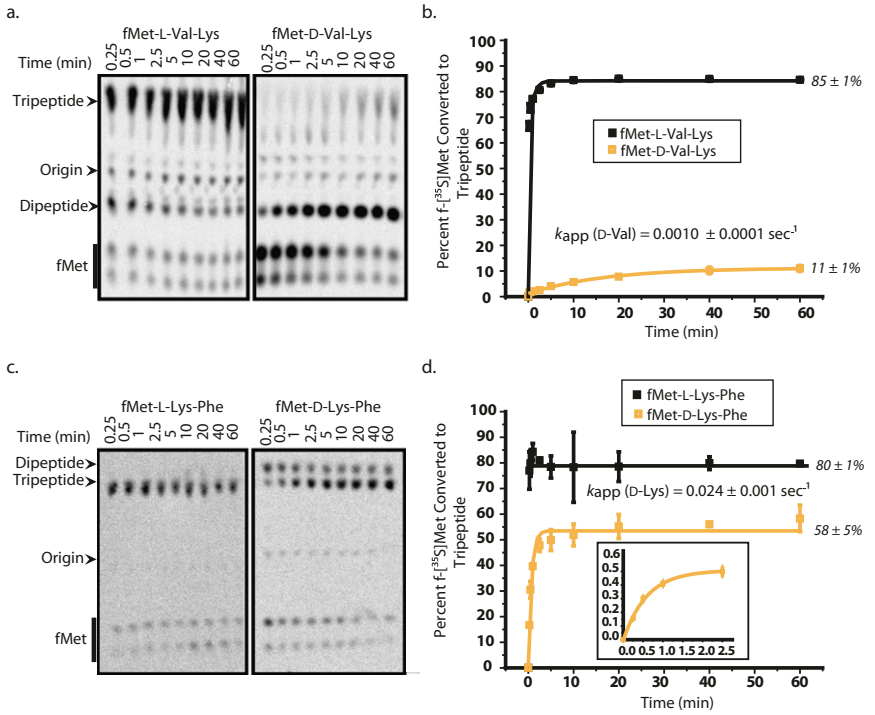

Fig. S4. D-Val-tRNA^{Val} and D-Lys-tRNA^{Lys} inhibit tripeptide synthesis by the TM in a manner that is analogous to that which is observed for D-Phe-tRNA^{Phe}. (*A*) eTLC analyses of f-[^{35}S]-Met-D/L-Val-Lys and (*C*) f-[^{35}S]-Met-D/L-Lys-Phe tripeptide synthesis reactions. Plots of the percent f-[^{35}S]-Met converted to tripeptide as a function of time for (*B*) f-[^{35}S]-Met-D/L-Val-Lys and (*D*) f-[^{35}S]-Met-D/L-Lys-Phe tripeptide synthesis reactions. Experiments were run in duplicate, and the SE is reported. These experiments demonstrate that D-Val-tRNA^{Val} and D-Lys-tRNA^{Lys} both inhibit tripeptide synthesis by the TM in a manner that is analogous to that which is observed for D-Phe-tRNA^{Phe}, resulting in the conversion of only 11% or 58% of f-[^{35}S]-Met into tripeptide, respectively.

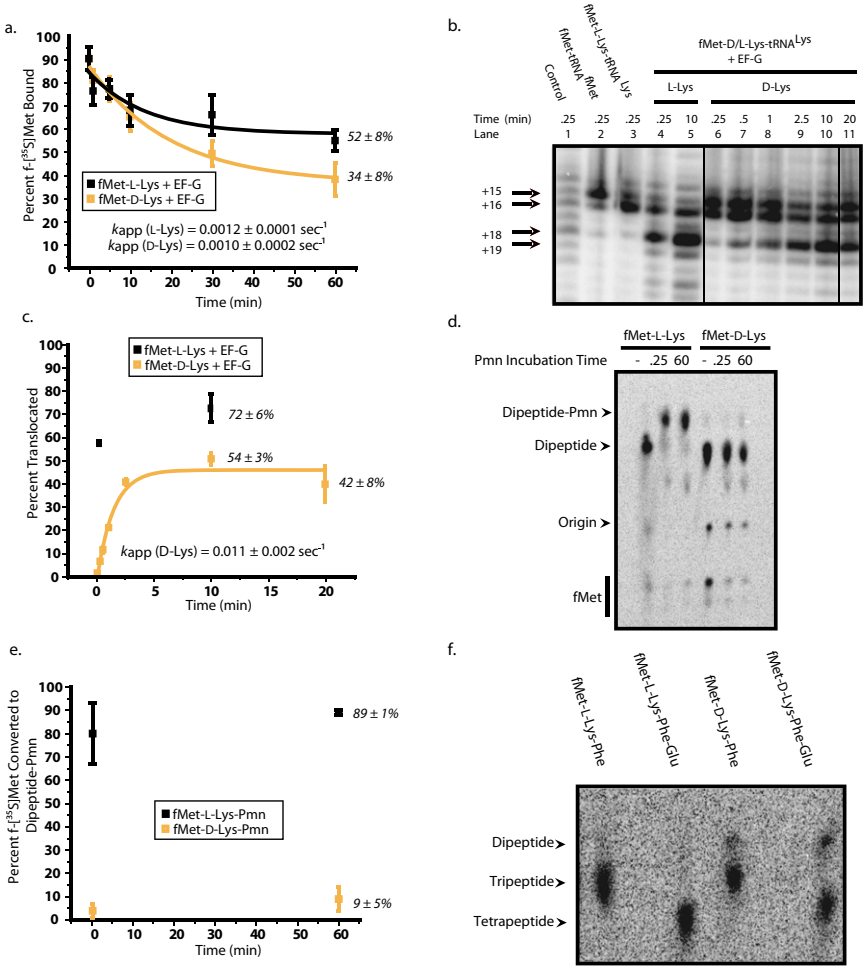

Fig. S5. During continuous translation, fMet-D-Lys-tRNA^{Lys} arrests translation in a smaller subpopulation of ECs than that which is observed for fMet-D-Phe-tRNA^{Phe}. (*A*) Nitrocellulose filter binding assays demonstrate that f-[^{35}S]-Met-D-Lys-tRNA^{Lys} remains stably bound to ECs during the course of f-[^{35}S]-Met-D-Lys-Phe tripeptide synthesis. These experiments were performed in triplicate, and the SD is reported. (*B* and *C*) Toeprinting assays reveal that fMet-D-Lys-tRNA^{Lys} is translocated from the A site to the P site of the ECs with a yield of 54%. This is slightly lower than the 72% translocation yield that is observed for the translocation of fMet-L-Lys-tRNA^{Lys}. This observation indicates that, in addition to arresting the PTC, A site-bound fMet-D-Lys-tRNA^{Lys} might also slightly interfere with translocation. Experiments were run in duplicate, and the SE is reported. The black vertical lines within the gel image denote where separate image segments taken from the same raw gel image were spliced together to generate the final gel image. (*D* and *E*) Pmn reactions demonstrate that only 9% of f-[^{35}S]-Met is converted to f-[^{35}S]-Met-D-Lys-Pmn. This is significantly less than the 58% conversion of f-[^{35}S]-Met to f-[^{35}S]-Met-D-Lys-Phe that is observed in tripeptide synthesis reactions (Fig. S4 *C* and *D*). Experiments were run in duplicate, and the SE is reported. (*F*) Tetrapeptide synthesis reactions demonstrate that the tripeptide containing fMet-D-Lys-Phe is competent for a further round of elongation. Collectively, these results demonstrate that, during continuous translation, ECs carrying P site-bound fMet-D-Lys-tRNA^{Lys} partition into translationally competent and translationally arrested subpopulations and strongly suggest that translation arrest arises from a significant defect in the ability of the D-Lys at the C terminus of the fMet-D-Lys-tRNA^{Lys} to participate as a donor in the peptidyl-transferase reaction. Interestingly, the difference between the 58% yield of fMet-D-Lys-Phe obtained in the tripeptide synthesis reactions and the 9% yield of fMet-D-Phe-Pmn obtained in the Pmn reactions additionally suggests that the nature of the incoming A-site substrate (i.e., Phe-tRNA^{Phe} vs. Pmn) can further modulate the ability of the D-Lys at the C terminus of the fMet-D-Lys-tRNA^{Lys} to participate as a donor in the peptidyl-transferase reaction.

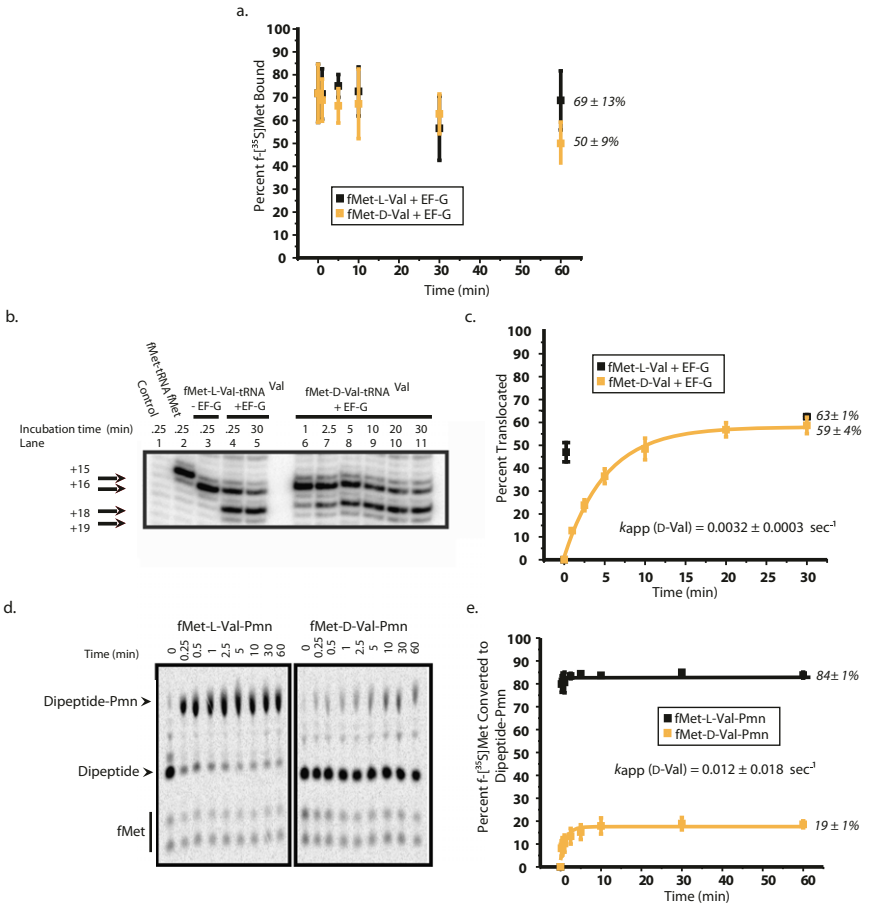

Fig. S6. During continuous translation, fMet-D-Val-tRNA^{Val} arrests translation in a larger subpopulation of ECs than that which is observed for fMet-D-Phe-tRNA^{Phe}. (*A*) Nitrocellulose filter binding assays demonstrate that f-[^{35}S]-Met-D-Val-tRNA^{Val} remains stably bound to ECs during the course of f-[^{35}S]-Met-D-Val-Lys tripeptide synthesis. Experiments were run in triplicate, and the SD is reported. (*B* and *C*) Toeprinting assays reveal that fMet-D-Val-tRNA^{Val} is translocated from the A site to the P site of the ECs with a yield of 59%. This is in close agreement with the yield of 63% that is observed for the translocation of fMet-L-Val-tRNA^{Val}. Experiments were run in duplicate, and the SE is reported. (*D* and *E*) Pmn reactions demonstrate that 19% of f-[^{35}S]-Met is converted to f-[^{35}S]-Met-D-Val-Pmn. This is in close agreement with the 11% conversion of f-[^{35}S]-Met to f-[^{35}S]-Met-D-Val-Lys observed in tripeptide synthesis reactions (Fig. S4 *A* and *B*). Experiments were run in duplicate, and the SE is reported. Tetrapeptide synthesis reactions involving D-Val-tRNA^{Val} could not be analyzed due to the low yields of the tri- and tetrapeptide products and/or because of an inability to resolve the tetrapeptide product from the other peptide products. Collectively, these results demonstrate that, during continuous translation, ECs carrying P site-bound fMet-D-Val-tRNA^{Val} partition into translationally competent and translationally arrest subpopulations, strongly suggesting that the observed translation arrest arises from a significant defect in the ability of the D-Val at the C terminus of the fMet-D-Val-tRNA^{Val} to participate as a donor in the peptidyl-transferase reaction.

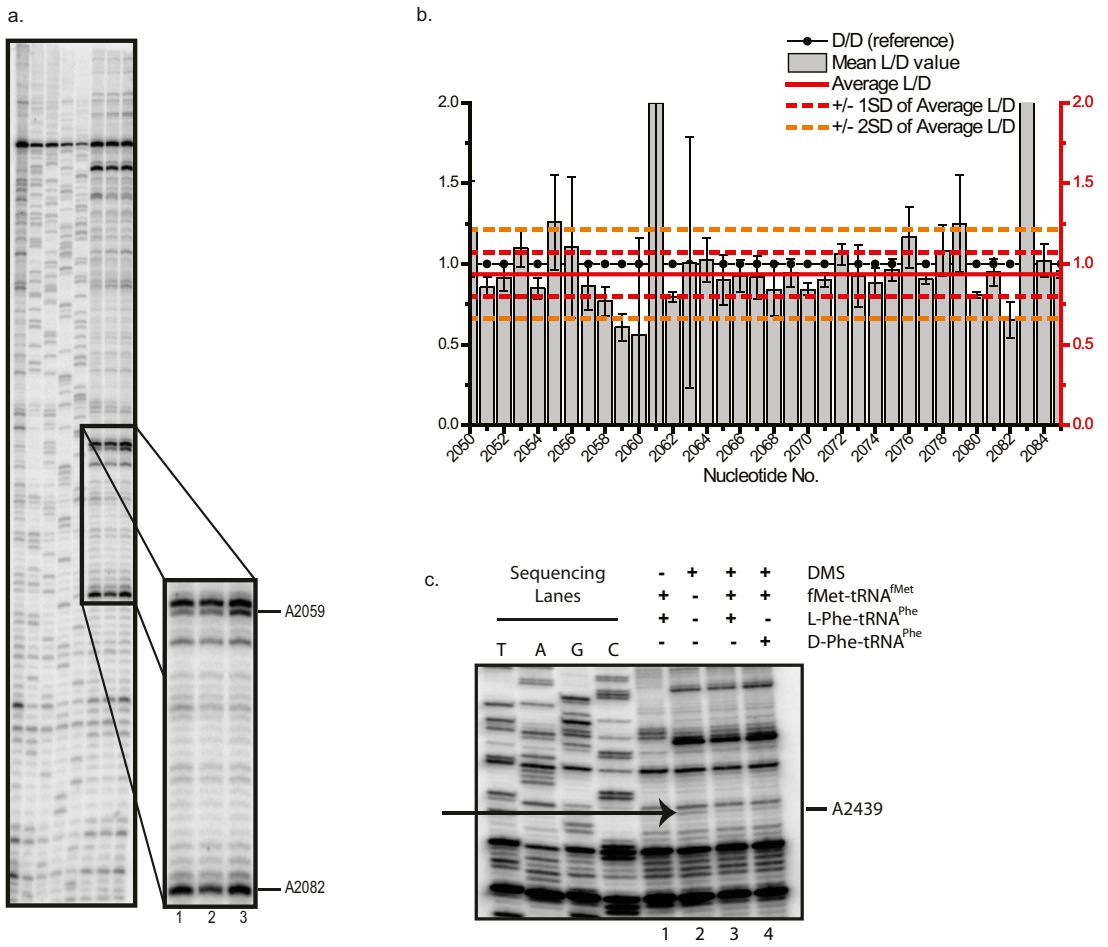

Fig. S7. Statistical analysis of chemical probing data. (*A*) A representative d-PAGE gel comparing the DMS modification pattern of rRNA nucleotides of ECs containing either a P site-bound fMet-L-Phe-tRNA^{Phe} or fMet-D-Phe-tRNA^{Phe}. The [^{32}P]-labeled cDNA products generated by reverse transcription of DMS-treated ribosomes were separated by d-PAGE gel and analyzed for the extent of modification of individual nucleotides, as described in *Chemical Probing Experiments*. Lane 1 contains vacant ribosomes treated with DMS. Lane 2 contains DMS-modified ECs carrying P site-bound fMet-L-Phe-tRNA^{Phe} treated with DMS. Lane 3 contains DMS-modified ECs carrying P site-bound fMet-D-Phe-tRNA^{Phe}. rRNA nucleotides A2059 and A2082 were identified as exhibiting a large change in the extent of modification depending on whether ribosomes were complexed with P site-bound fMet-L-Phe-tRNA^{Phe} (lane 2) or P site-bound fMet-L-Phe-tRNA^{Phe} (lane 3). Experiments were performed in triplicate. (*B*) Statistical analysis of chemical probing d-PAGE gels. The band intensities for each rRNA nucleotide (2050–2085) from three independent chemical protection experiments were analyzed using SAFA software, and further data analysis was done as described in *Chemical Probing Experiments*. Gray bars depict the mean L/D intensity value for each nucleotide, and the corresponding black error bars depict the SD from the mean. The solid red line corresponds to the average L/D ratio of all gel nucleotides. The solid black line connecting filled black circles denotes the D/D ratio, which is a reference value. Dashed red lines correspond to ±1 SD from the mean, and dashed orange lines correspond to ±2 SDs from the mean. A change in nucleotide accessibility was considered statistically significant if the extent of modification was at least ±2 SDs from the average. (*C*) To confirm that acylated tRNA was indeed present and that the P site was occupied during the chemical probing experiments, we looked for changes in the DMS modification of 23S rRNA nucleotide A2439, a nucleotide that is known to be exposed to DMS in vacant ribosomes but that is protected from DMS in ECs carrying a P-site peptidyl-tRNA (1). Comparison of the accessibility of A2439 to DMS modification in vacant ribosomes (lane 2) versus in ECs carrying fMet-L-Phe-tRNA^{Phe} at the P site (lane 3) or fMet-D-Phe-tRNA^{Phe} at the P site (lane 4) demonstrates that the accessibility of A2439 to DMS modification is reduced in both ECs relative to its accessibility in vacant ribosomes, thereby suggesting that both ECs contain a P-site tRNA.

1. Moazed D, Noller HF (1989) Interaction of tRNA with 23S rRNA in the ribosomal A, P, and E sites. *Cell* 57(4):585–597.

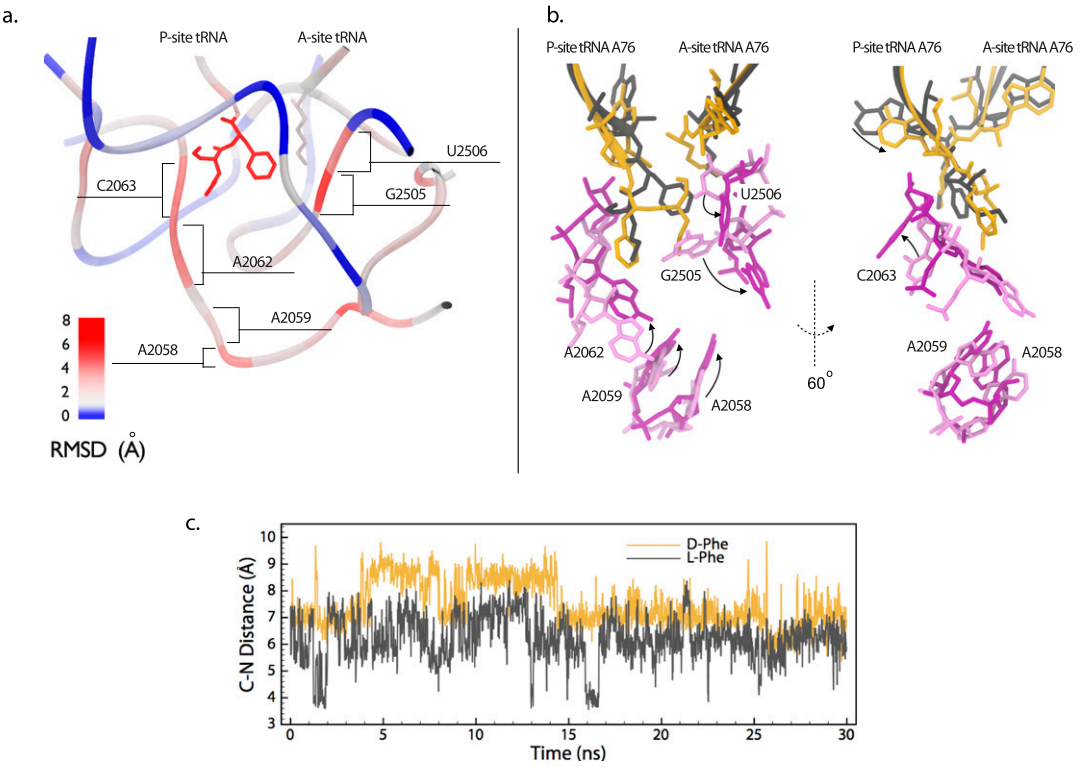

Fig. S8. Structural comparison of the PTC core of ECs carrying either fMet-D-Phe-tRNA^{Phe} or fMet-L-Phe-tRNA^{Phe} at the P site. (*A*) Per-residue root mean square displacement (RMSD) values between the average structures of ECs carrying either fMet-L-Phe-tRNA^{Phe} or fMet-D-Phe-tRNA^{Phe} in the P site are color-coded and shown using a trace representation of the fMet-L-Phe-tRNA^{Phe} EC, and only structures within 15 Å of the P-site dipeptidyl-tRNA are shown. (*B*) Nucleotides with large structural differences are shown in stick representations, colored as in Fig. 3*B*. (*C*) Changes in the C–N distances as a function of time for ECs carrying either P site-bound fMet-L-Phe-tRNA^{Phe} (shown in black) or fMet-D-Phe-tRNA^{Phe} (shown in gold) and A site-bound Lys-tRNA^{Lys}. C–N distances refer to the distance between the electrophilic carbonyl carbon (C) atom of the C-terminal amino acid that is esterified to the P site-bound peptidyl-tRNA and the nucleophilic α-amine nitrogen (N) atom of the amino acid that is esterified to the A site-bound aa-tRNA.

Table S1. Fitting parameters, rates, and endpoints for experimental data*

Experiment	A_1, %†	τ_1, min†	y_0, %†	R^{2}†	k_{app}, s^{-1}‡	Endpoint, %§
fMet-D-Phe dipeptide	−73.56	0.84	77.94	0.97	0.020 ± 0.004	81 ± 3
fMet-D-Val dipeptide	−81.86	3.18	84.70	0.99	0.0052 ± 0.0004	87 ± 1
fMet-D-Lys dipeptide	−75.56	0.34	76.82	0.98	0.05 ± 0.01	81 ± 5
fMet-D-Phe-Lys tripeptide	−17.05	3.79	17.14	0.99	0.004 ± 0.001	18 ± 3
fMet-D-Val-Lys tripeptide	−10.01	17.01	11.21	0.98	0.0010 ± 0.0001	11 ± 1
fMet-D-Lys-Phe tripeptide	−52.71	0.69	53.49	0.98	0.024 ± 0.001	58 ± 5
fMet-D-Phe filter binding	45.19	61.96	34.70	0.97	0.0003 ± 0.0003	34 ± 8
fMet-L-Phe filter binding	24.78	33.76	56.82	0.99	0.0005 ± 0.0003	52 ± 8
fMet-D-Val filter binding	N/D¶	N/D¶	N/D¶	N/D¶	N/D¶	50 ± 9
fMet-L-Val filter binding	N/D¶	N/D¶	N/D¶	N/D¶	N/D¶	65 ± 13
fMet-D-Lys filter binding	28.61	13.73	55.09	0.83	0.0010 ± 0.0002	34 ± 8
fMet-L-Lys filter binding	24.19	21.08	53.71	0.87	0.0012 ± 0.0001	52 ± 8
fMet-D-Phe toeprinting	−77.08	0.87	77.20	0.99	0.019 ± 0.001	78 ± 5
fMet-D-Val toeprinting	−56.70	5.15	58.01	0.99	0.0032 ± 0.0003	59 ± 4
fMet-D-Lys toeprinting	−50.64	1.46	48.71	0.96	0.011 ± 0.002	42 ± 8
fMet-D-Phe Pmn	−16.04	0.18	16.20	0.92	0.09 ± 0.08	18 ± 1
fMet-D-Val Pmn	−14.66	1.38	17.59	0.91	0.012 ± 0.018	19 ± 1

*All data were fit to the following equation using Origin 7: $y = A_1(e^{-x/\tau 1}) + y_0$.

†Reported fitting parameters were obtained by plotting and fitting the average of each time point in two (dipeptide, tripeptide, and Pmn) or three (filter binding) experimental trials.

‡The error for the k_{app} was calculated in the following manner. First, each of the two runs were plotted and fit to the above equation, generating individual τ_1 values and individual k_{app}s for each run. The SE from these k_{app}s is reported.

§The 60-min time points for each of the two (dipeptide, tripeptide, and Pmn) or three (filter binding) experimental trials were averaged to determine the endpoint. The SE is reported for experiments with two trials, and the SD is reported for experiments with three trials.

¶The change in percent f-[^{35}S]-Met-Val-tRNA^{Val} bound to ribosomes changes very little as a function of time during our observation period (60 min). Therefore, we were unable to accurately fit these data to an experimental decay function.

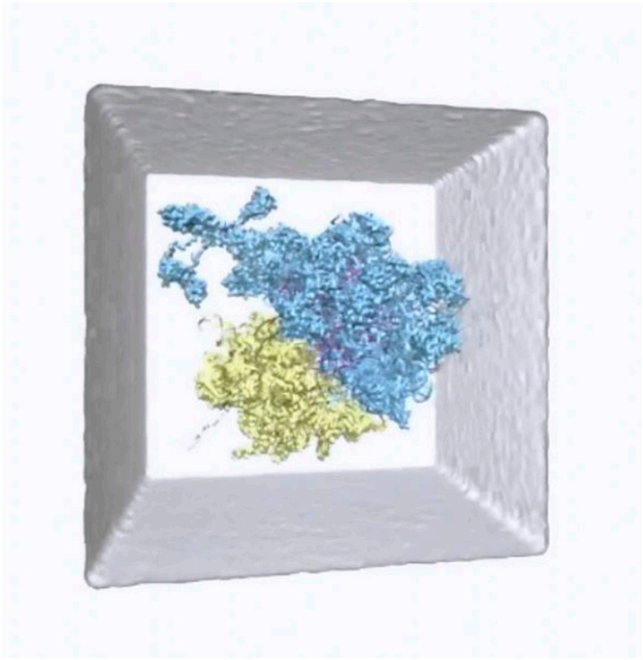

Movie S1. Two MD simulations of ECs carrying either P site-bound fMet-L-Phe-tRNA^{Phe} (shown in black) or a P site-bound fMet-D-Phe-tRNA^{Phe} (shown in gold) were superimposed. PTC nucleotides for the superimposed ECs are shown in light purple (P site-bound fMet-L-Phe-tRNA^{Phe}) and dark purple (P site-bound fMet-D-Phe-tRNA^{Phe}).

Movie S1